Nonaqueous gas diffusion electrodes for rapid ammonia synthesis from nitrogen and water splitting-derived hydrogen

Nikifar Lazouski,[1] Minju Chung,[1] Kindle Williams,[1] Michal L. Gala,[1] and Karthish Manthiram[1*]

[1]Department of Chemical Engineering; Massachusetts Institute of Technology; Cambridge, MA 02139, USA.

*Correspondence to: karthish@mit.edu

Abstract: Electrochemical transformations in nonaqueous solvents are important for synthetic and energy storage applications. Use of nonpolar gaseous reactants such as nitrogen and hydrogen in nonaqueous solvents is limited by their low solubility and slow transport. Conventional gas diffusion electrodes improve transport of gaseous species in aqueous electrolytes by facilitating efficient gas-liquid contacting in the vicinity of the electrode. Their use with nonaqueous solvents is hampered by the absence of hydrophobic repulsion between the liquid phase and carbon fiber support. Herein, we report a method to overcome transport limitations in tetrahydrofuran using a stainless steel cloth-based support for ammonia synthesis paired with hydrogen oxidation. An ammonia partial current density of 8.8±1.4 mA cm^{-2} and a Faradaic efficiency of 35±6% are obtained using a lithium-mediated approach. Hydrogen oxidation current densities up to 25 mA cm^{-2} are obtained in two nonaqueous solvents with nearly unity Faradaic efficiency. The approach is then applied to produce ammonia from nitrogen and water splitting-derived hydrogen.

Introduction

Electrochemical synthesis of chemicals is an attractive alternative approach to traditional thermochemical methods. In some reactions, electric potential can act as a thermodynamic driving force instead of high temperatures and pressures, which may allow for operation at milder conditions and in a modular fashion.[1,2] Ammonia (NH_3) production is an example of a reaction that may benefit from being operated electrochemically.[3,4] NH_3 is currently produced predominantly via the Haber-Bosch process, which operates at high temperatures (300-500 °C) and pressures (200-300 bar) and requires a coupled steam reforming plant for hydrogen (H_2) production.[5] This leads to high capital costs for the process and centralization of production, a situation that is poorly matched with the distributed nature of ammonia utilization.[6] Alternative methods for producing hydrogen, such as water splitting, may overcome some of the issues associated with the traditional Haber-Bosch process, such as the large amount of CO_2 emissions and high capital cost associated with steam reforming.[7] However, these methods do not overcome the need for large scales for the ammonia synthesis reactor itself, as it must still be run at high temperatures and pressures. An electrochemical process – even one which utilizes multiple reactors – that produces ammonia from nitrogen and water requires a thermodynamic minimum potential of 1.17 V at standard conditions.[4] Potential is a potent thermodynamic driver, providing mild conditions conducive to modular and small-scale operation of electrochemical processes.[8]

Despite the attractiveness of electrochemistry in synthetic applications, several challenges must be overcome to allow for efficient scale-up of the technology. One of the most important issues is the use of non-renewable reactants at the counter electrode. For reductive chemistries, which are important for energy storage and certain synthetic applications,[9–12] the counter reaction is often oxidation of solvent or sacrificial anodes made of active metals.[13,14] In aqueous systems, solvent oxidation is permissible and often desired. However, oxidation of organic solvents or

sacrificial anodes decreases the atom economy of reactions greatly and makes processes utilizing these reactions poorly amenable to continuous operation.[13]

In the context of nitrogen reduction, one method that produces ammonia at high rates and Faradaic efficiencies (FEs) is the lithium-mediated approach. The approach involves reacting lithium metal with nitrogen to form lithium nitride, a reaction which is spontaneous at ambient conditions. The lithium nitride is then protonated to make ammonia and a lithium salt. The lithium salt is electrochemically reduced to lithium metal to close the catalytic cycle (Fig. 1a). The efficacy of the chemistry has been demonstrated in batch processes in which the aforementioned reactions are run with temporal separation; mostly they differ primarily in the method used to generate lithium metal.[15–18] While these processes demonstrate high Faradaic efficiencies, they are not directly amenable to continuous ammonia production, though approaches to utilize rotating reactors for a pseudo-continuous process have been proposed.[19] In this regard, continuous processes in which all three reactions happen simultaneously are attractive. Typically, continuous processes utilize a lithium salt in tetrahydrofuran (THF) electrolyte with ethanol as a proton source.[20–23] While the cathode reactions in this system are well-described (Fig. 1a), the anode reaction is poorly defined and likely involves THF oxidation. Solvent decomposition prevents the method from being a practical approach to ammonia production.

Oxidizing H_2 at the anode to produce protons of a controlled thermodynamic activity avoids the aforementioned issues.[24] As an added benefit, hydrogen oxidation can be used as a renewable anode reaction for synthetic applications in which sacrificial anodes are used, allowing for continuous production of useful chemicals.[13] However, the rate of hydrogen oxidation in nonaqueous solvents at flooded electrodes is limited by the solubility of hydrogen[25] and its corresponding diffusion-limited oxidation rate,[26] equal to several milliamperes per square

centimeter (mA cm^{-2}) (Fig. 1b), which is far too low for practical applications.[4] Similar diffusion limitations are pronounced for gaseous feedstocks such as N_2 (Fig. 1c).[20,27]

One way to overcome diffusion limitations for gaseous reactants in electrochemical reactions is to use gas diffusion electrodes (GDEs), in which intimate contact between the gas, electrolyte, and catalyst is generated.[28] This contacting minimizes the distance that gas molecules have to travel through the electrolyte to react at the catalyst (Fig. 2a), thus achieving much higher diffusion rates than are possible at flooded electrodes in aqueous electrolytes. GDEs have been used in hydrogen fuel cells[28,29] and for CO[30] and CO_2 reduction.[31–33]

In the aforementioned applications, the electrolytes are typically aqueous solutions or water-saturated polymeric materials, while the GDE support is hydrophobized to control wetting.[28] The hydrophobic interactions between the electrolyte and support, as well as the small pore size in the support prevent electrolyte penetration and flooding into the fibrous structure of the GDE. Instead, a thin layer of electrolyte is in contact with the catalyst through which reactant gas molecules must diffuse (Fig. 2a).[34] If the primary component of the electrolyte is a nonaqueous solvent, such as tetrahydrofuran (THF), then the interactions between the support and electrolyte are no longer unfavorable, which leads to penetration of the electrolyte into the fibrous structure of the GDE (Fig. 2b), effectively flooding the catalyst. The gas must then diffuse over large distances through the solution to react (Fig. 2b), lowering the maximum obtainable current densities.[35] Flooding prevents the use of standard carbon fiber-based GDEs with nonaqueous electrolytes for improving the rates of reactions involving sparingly soluble gases. While some approaches to overcome these issues have been reported,[35–37] to the best of our knowledge, no previously reported GDE generated effective gas-liquid contact to greatly increase the obtained current for electrosynthetic applications in nonaqueous solvents.

In the present work, we were able to obtain GDE-like behavior by controlling material wetting and electrolyte penetration into supports when using nonaqueous electrolytes. We used a stainless steel cloth (SSC) as the substrate onto which the catalyst was deposited. Electrolyte penetration was controlled by maintaining a pressure gradient across the cloth. The approach was used to efficiently oxidize H_2 on Pt-coated steel cloths (Pt/SSC) at current densities up to 25 mA cm^{-2} in tetrahydrofuran and propylene carbonate-based electrolytes. In addition, by using an SSC as a substrate onto which lithium metal is plated in situ, we were able to reduce N_2 to NH_3 using a lithium-mediated approach. An NH_3 partial current density of 8.8±1.4 mA cm^{-2} and high FEs (35±6% at rate-optimized conditions, 47.5±4% at FE-optimized conditions) were obtained. The two electrodes were coupled to build an electrochemical Haber-Bosch (eHB) reactor, which can produce NH_3 from N_2 and H_2 at ambient conditions.

Results

Carbon fiber electrodes for hydrogen oxidation

First, we sought to improve the rates of the hydrogen oxidation reaction (HOR) in a THF-based electrolyte in order to utilize it as a renewable anode chemistry. Initially, we attempted to use commercially available platinum on carbon fiber (Pt/C) GDEs, which are capable of greatly increasing the rate of hydrogen oxidation in aqueous electrolytes (Supplementary Fig. 1). When flowing H_2 gas past the GDEs with a THF-based electrolyte we found that very little H_2 oxidation occurs at any applied current (Fig. 3a). Establishing a large (20 kPa) pressure gradient across the GDE to allow gas flow through the GDE in order to prevent complete flooding improved HOR FE somewhat (Fig. 3a). The pressure gradient at which flow through the GDE is observed is defined by the Laplace pressure;[38] it was found to be 20±4 kPa for Pt/C GDEs. At pressure gradients at which gas flow through the electrode is observed, commercially available Pt/C GDEs were able to

support HOR partial current density of ~12 mA cm^{-2} (Fig. 3a), estimated by taking the product of the total applied current and measured HOR FE.

Stainless steel cloth electrodes for hydrogen oxidation

The fibrous structure of Pt/C GDEs and favorable interactions between the nonaqueous electrolyte and carbon are responsible for flooding of the electrode (Fig. 2b, Supplementary Fig. 2). The flooding behavior makes Pt/C GDEs unsuitable for high rate gas utilization. Therefore, we sought to use an alternative GDE support to avoid these issues. We chose stainless steel cloths (SSC) as the GDE support (Fig. 2c, Extended Data Fig. 1a), as, unlike carbon fibers, metal threads do not take up electrolyte by capillary action (Supplementary Fig. 2). At non-zero pressure gradients across the SSC, a well-defined separation between the gas and liquid is obtained (Supplementary Fig. 2). As stainless steel is a poor hydrogen oxidation catalyst, we electrodeposited platinum (Supplementary Figs. 3-7), which is an active HOR catalyst, onto the stainless steel cloths. The platinum-coated steel cloths (Pt/SSC) are able to oxidize H_2 in the THF-based electrolyte with nearly unity FE (Fig. 3a) up to applied current densities of 25 mA cm^{-2}; higher current densities were difficult to test due to large electrolyte resistance. This corresponds to approximately one order of magnitude increase in the HOR current when compared to a flooded geometry (Fig. 1b). Hydrogen oxidation was confirmed by cyclic voltammetry experiments (Supplementary Fig. 8) and by accounting for the hydrogen mass balance (Supplementary Fig. 9). The increase in the maximum rate of HOR cannot be explained by a simple electroactive surface area effect, as a higher surface area electrode flooded by electrolyte would be subject to the same one dimensional transport-limited current density.[26] The breaking of this transport limitation can result in increases in current; this breaking arises from the establishment of gas-liquid interfaces which promote gas transport close to the electrode surface.

The HOR FE demonstrates robustness to changes in non-zero pressure gradients across the Pt/SSC (Fig. 3b). Pressure gradients at or above the Laplace pressure of the cloth, which is 1.9±0.2 kPa for Pt/SSC, lead to gas flow into the electrolyte (Supplementary Fig. 2).[38] While gas flow through the electrode into the electrolyte does not affect the SSC performance, it may be undesirable for continuous operation due to the need to control multiple gas streams in the electrochemical cell. By maintaining the pressure gradient below the Laplace pressure of the cloth, gas flow exclusively past the electrode can be achieved. A majority of the experiments described in this work were performed with gas flow past the electrode. At non-zero pressure gradients across the Pt/SSC, the flowrate of H_2 past the electrode can be varied with no change in HOR FE (Supplementary Fig. 10). At the highest applied currents and lowest flowrates, the nominal single pass conversion of hydrogen is approximately 80% (Supplementary Fig. 10), which is significantly higher than the single pass conversion of 25-35% used in traditional Haber-Bosch reactors.[39]

In order to demonstrate the generality of the approach of using SSC as a GDE support for nonaqueous solvents, we attempted to oxidize hydrogen at high rates in a 1 M $LiBF_4$ in 9:1 propylene carbonate:dimethyl carbonate electrolyte. The electrolyte is similar to electrolytes used in some batch lithium-mediated nitrogen reduction approaches.[16,17] We found that the transport-limited hydrogen oxidation current density at flooded Pt foil electrodes is ~0.25 mA cm^{-2} (Supplementary Fig. 11), which is an order of magnitude lower than for hydrogen oxidation in THF-based electrolyte (Fig. 1b), likely due to the propylene carbonate electrolyte's higher viscosity and lower hydrogen solubility. By using a Pt/SSC anode, we were able to oxidize hydrogen at rates of 25 mA cm^{-2} with near unity FE in the propylene carbonate-based electrolyte (Supplementary Fig. 11). These current densities are two orders of magnitude higher than in the flooded case, even despite an absence of good proton acceptors in the electrolyte. This experiment

demonstrates that SSCs can be used to obtain GDE-like behavior across different nonaqueous solvents.

Stainless steel cloth electrodes for nitrogen reduction

Having overcome transport limitations for hydrogen oxidation by using SSCs as anodes, we sought to implement SSCs for the cathodic reaction of nitrogen reduction. The lithium metal-mediated approach for N_2 reduction has been reported to be diffusion limited in THF on flooded copper and steel foils (Fig. 1c).[20] In aqueous electrolytes, the transport limited current density for nitrogen reduction is typically even lower than in nonaqueous systems – approximately 0.5-1.3 mA cm^{-2} – and depends on the hydrodynamics of the electrolyte (see Supplementary Discussion). The transport limited current density can be increased by decreasing the boundary layer thickness through improving the hydrodynamics, for instance with a rotating disk electrode (RDE) or microfluidic reactor, or by using gas diffusion electrodes. Claims of nitrogen reduction in aqueous electrolytes above these rates that do not utilize methods to improve nitrogen transport must be examined with scrutiny, adding an additional criterion for evaluating the veracity of nitrogen reduction reports.[21,40]

To overcome diffusion limitations, we used a stainless steel cloth (SSC) as the GDE substrate onto which lithium metal was plated in situ. We found that the rate of the nitrogen reduction reaction (NRR) is significantly enhanced compared to the flooded case (Fig. 1c) at high applied currents (Fig. 3c). This enhancement demonstrates that SSC cathodes can yield rates for continuous NRR that are competitive with literature reports (Fig. 4a, Supplementary Table 1). At the highest production rates (Fig. 3c), a total of 8.7±1.4 μmol of ammonia are produced at a 1 cm^2 electrode after 290 seconds of polarization, resulting in 4.5±0.6 mM and 0.46±0.22 mM ammonia concentrations in the electrolyte and trap, respectively. At the highest FEs (Fig. 3d), a total of

11.8±1 μmol of ammonia are produced after 480 seconds of polarization. As the total amount of charge passed in most experiments was constant and equal to 7.2 coulombs, current was applied to the cell for longer periods of time than 290 seconds in most experiments. In longer duration experiments in which more charge was passed, 102 μmol of ammonia were produced over the course of 130 minutes, with an FE of 18.9% (Supplementary Fig. 12). We found that the total amount of ammonia produced increases monotonically with time after an induction period of approximately 2 minutes (Supplementary Fig. 13), which suggests that the lithium-based catalyst cycle (Fig. 1a) rapidly reaches steady state operation. As the induction period is included in the time used to compute production rates, the rates reported here are underestimates of true values for a continuous system. Longer duration experiments (Supplementary Fig. 12) suggest that the production rate decreases with time, which could occur for a number of reasons, including but not limited to lithium ion depletion, solution phase ammonia affecting lithium plating and nitridation reactions, and incomplete proton donor recycling. Further experiments are necessary to conclusively determine and address the cause of the decreasing ammonia production rate at longer times.

Nitrogen reduction control experiments

We confirmed that NH_3 is produced via N_2 reduction by performing control experiments in which argon and isotopically labelled N_2 were used as feed gases (Extended Data Fig. 2).[21,40] No NH_3 is produced with argon as a feed gas, and there is quantitative agreement between the amount of NH_3 produced when $^{14}N_2$ and $^{15}N_2$ are used as feed gases.[21] The isotope labeling experiments were performed at two different operating conditions and architectures, which is necessary for conclusive proof of nitrogen reduction.[41] The produced NH_3 can be found in both the solution and the gas phases (Fig. 3c, d). This is additional evidence of GDE-like behavior of

the SSC cathode. Obtaining ammonia in the gas phase is desirable as it may simplify separations in a practical process.

In the absence of a pressure gradient across the SSC, the system reverts to a flooded state and generally shows poor efficiency for N_2 reduction (Fig. 3d). While the changes in total NH_3 FE with non-zero pressure gradients (Fig. 3d) do not demonstrate a clear trend when accounting for the measured uncertainty, a maximum average combined solution and gas phase FE of 47.5±4% was obtained when the pressure gradient was 0.5 kPa using a SSC as the cathode. The total NH_3 FE also does not significantly change when the flowrate of N_2 past the SSC is varied (Supplementary Fig. 10); less NH_3 is found in the gas phase at lower flowrates. The high conversions of N_2 (~10%) at low N_2 flowrates (Supplementary Fig. 10) are desirable for a practical process; they also are indirect evidence of N_2 reduction to NH_3, as the fraction of NO_x and NH_x impurities in the stock N_2 would need to be at approximately 1000-10000 parts per million to yield this much NH_3, several orders of magnitude higher than the maximum contamination levels of these impurities reported in the stock gas.

Demonstration of electrochemical Haber-Bosch

After obtaining efficient chemistries using SSCs independently at both the cathode and anode, we coupled the two reactions into an electrochemical Haber-Bosch (eHB) reactor, which produces NH_3 from N_2 and H_2 at ambient conditions. Using SSC-based GDEs for both electrodes in a single reactor (Fig. 2d), we maintained high ammonia yields at the cathode (Fig. 4b). At longer reaction times, the advantage of using H_2 oxidation at a Pt/SSC anode over THF oxidation at a platinum foil is evident, as solvent oxidation is avoided (Fig. 4b insets). The fate of the proton donor is also addressed by coupling the electrode chemistries. The proton donor, ethanol, is consumed at the cathode to produce NH_3 and ethoxide, and could be regenerated from the ethoxide

at the anode by protons produced from H_2 oxidation (Fig. 2d). In long duration experiments (Supplementary Fig. 12), the number of protons found in ammonia was ~80% of the number of labile protons originally present in ethanol in the electrolyte. As hydrogen evolution at the cathode also utilizes protons from ethanol, the high utilization of protons suggests that ethanol is indeed regenerated from ethoxide at the anode via hydrogen oxidation.

The eHB reactor operates at ambient conditions, which allows it to be operated at smaller scales than traditional Haber-Bosch.[4] However, H_2 is usually sourced from steam-methane reforming, which utilizes fossil fuels and is not readily modularized.[42] Water electrolysis is a modular alternative H_2 source. By coupling an electrochemical Haber-Bosch reactor and a water electrolyzer (Fig. 4c, d), we are able to obtain NH_3 in an overall reaction involving only N_2, H_2O, and renewable electrons. By using a commercially available water splitting setup, we were able to produce NH_3 with an FE of 30±2% (Fig. 4b). The slight decrease in FE compared to eHB is likely from water contamination from the H_2 stream. We believe that coupling multiple unit operations in series is advantageous for nonaqueous electrochemical ammonia production as it may increase the efficiency of each individual step as well as the overall process.

Conclusions

While development of GDEs capable of operating in nonaqueous solvents is imperative for practical electrochemical synthesis, many other aspects of system design require further development. Physical methods to recycle volatile organic solvents and separate the products when using gaseous feedstocks may be necessary in practical systems. Alternatively, bulk volatile solvents may be replaced with non-volatile analogs with similar properties, such as specially tailored polymers or ionic liquids. Polymeric electrolytes may open up avenues for manufacturing species-selective membranes for use in nonaqueous systems, analogous to Nafion in aqueous

systems, and for manufacture of membrane-electrode assemblies (MEAs) for gas phase reactions. Electrolyte engineering can also decrease the ionic resistance in the cell, which is important for energy efficiency at high currents.

In the current work, for instance, the energy efficiency for NH_3 production ranges from 1.4 to 2.8% at an applied cell potential of 20-30 V, with 70-80% of the energy losses coming from large electrolyte resistance (Supplementary Fig. 14). These values of energy efficiency correspond to energy consumptions of 730-1500 GJ/ton NH_3, significantly higher than contemporary values for Haber-Bosch, or even other lithium-mediated chemistries.[15] However, we believe that further improvements to the electrolyte, cell architecture, Faradaic efficiency and cell lifetime can greatly improve these metrics by reducing sources of energy loss (Supplementary Fig. 14).

This work demonstrates the possibility of utilizing metal cloth-based supports for high rate electrochemical reactions of sparingly soluble gaseous reactants in a nonaqueous solvent. We used these SSCs to produce ammonia from nitrogen and water-derived hydrogen at the highest reported rates at ambient conditions, 30±5 nmol cm^{-2} s^{-1} (Fig. 4a). The nonaqueous HOR Pt/SSC can find applications in reactions for which a continuous source of controlled-activity protons is needed, while an SSC at the cathode can be used in producing value-added chemicals from gaseous feedstocks such as N_2, CO_2, or CO. We believe this approach for utilizing gaseous reactants can become a staple of organic electrosynthetic methodology.

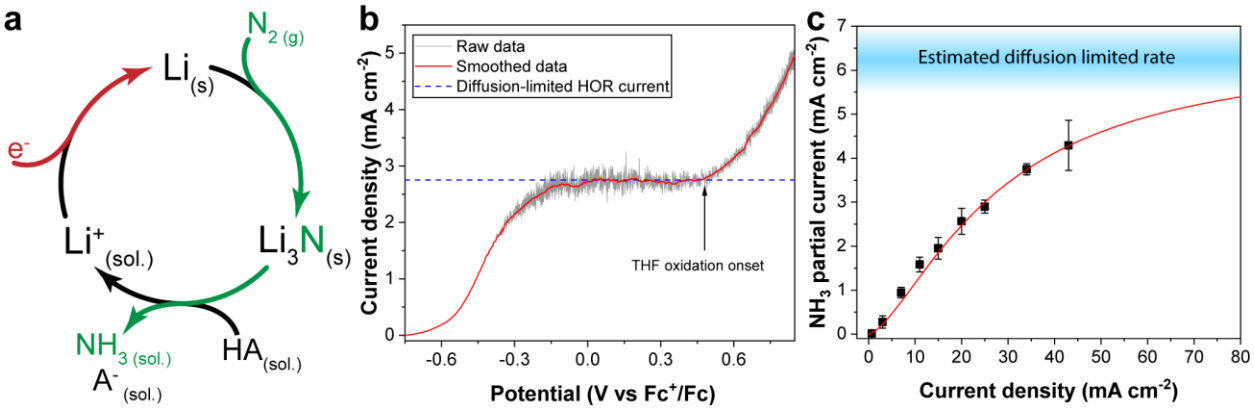

Fig. 1. Kinetic and transport considerations for lithium-mediated nitrogen reduction. (**a**) Reactions present in a lithium-mediated catalytic cycle for nitrogen reduction. (**b**, **c**) Diffusion limitations observed in electrochemical reactions involving sparingly soluble gases (**b**) hydrogen and (**c**) nitrogen in a 1 M $LiBF_4$, 0.11 M ethanol in tetrahydrofuran electrolyte at flooded platinum and steel electrodes, respectively. The data in (**b**) is collected by performing a linear sweep voltammogram at 5 mV s^{-1}. The blue line in (**b**) helps to guide the eye. The red line in (**c**) is a fit of the data to a kinetic-transport model for ammonia production.[20] Vertical error bars in (**c**) represent one standard deviation of multiple replicates of the same experiment ($n \geq 2$).

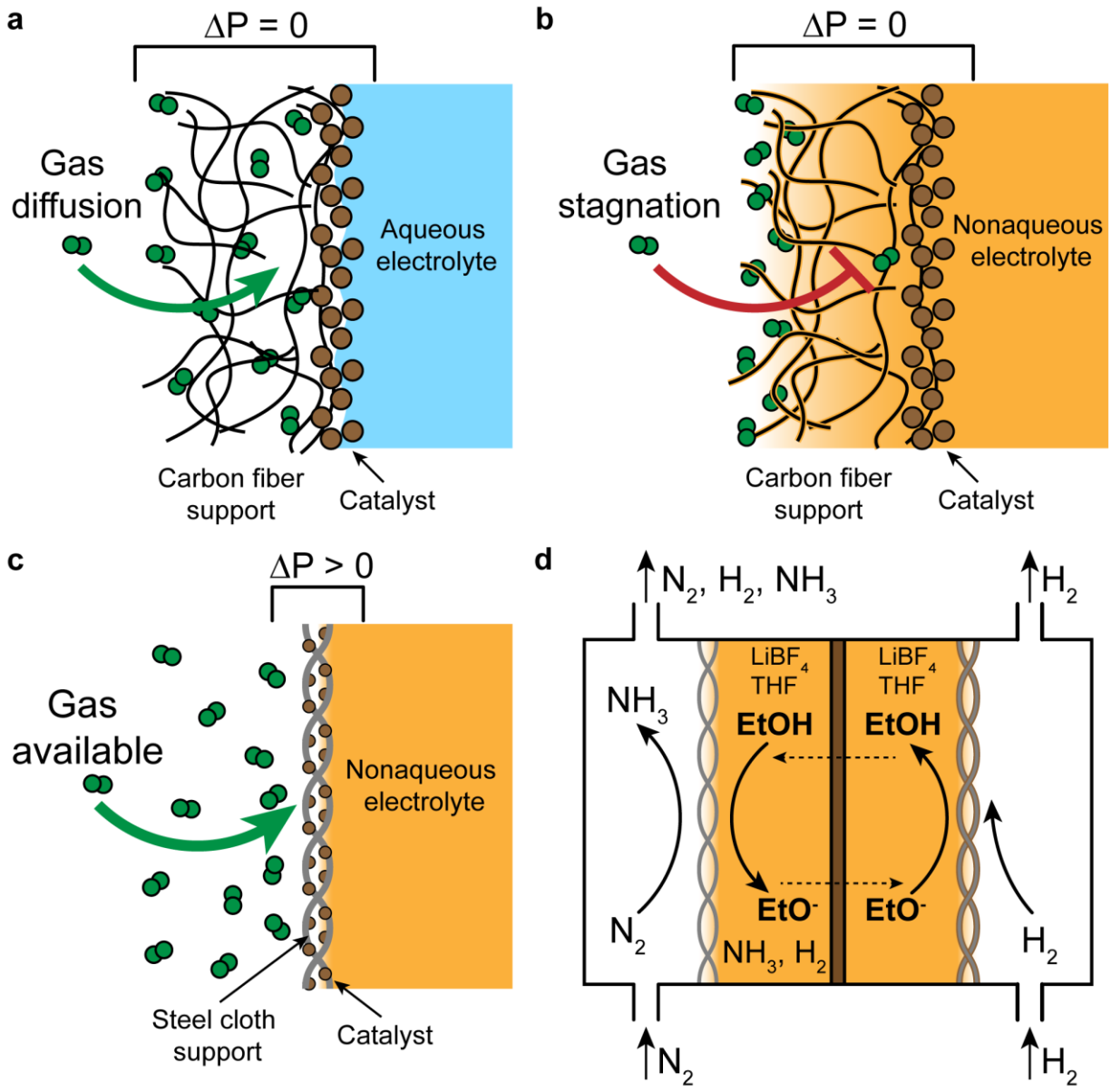

Fig. 2. Structure of a gas diffusion electrode (GDE). (**a**) A hydrophobic GDE with an aqueous electrolyte, where well-defined gas-liquid contacting exists. (**b**) A hydrophobic GDE with a nonaqueous electrolyte, where considerable wetting of the carbon fibers occurs, effectively flooding the catalyst. (**c**) A catalyst-coated steel cloth. A lack of significant capillary action and the presence of a non-zero pressure gradient across the cloth prevent complete catalyst flooding. (**d**) Proton donor cycling in a cell with a proton-producing anode.

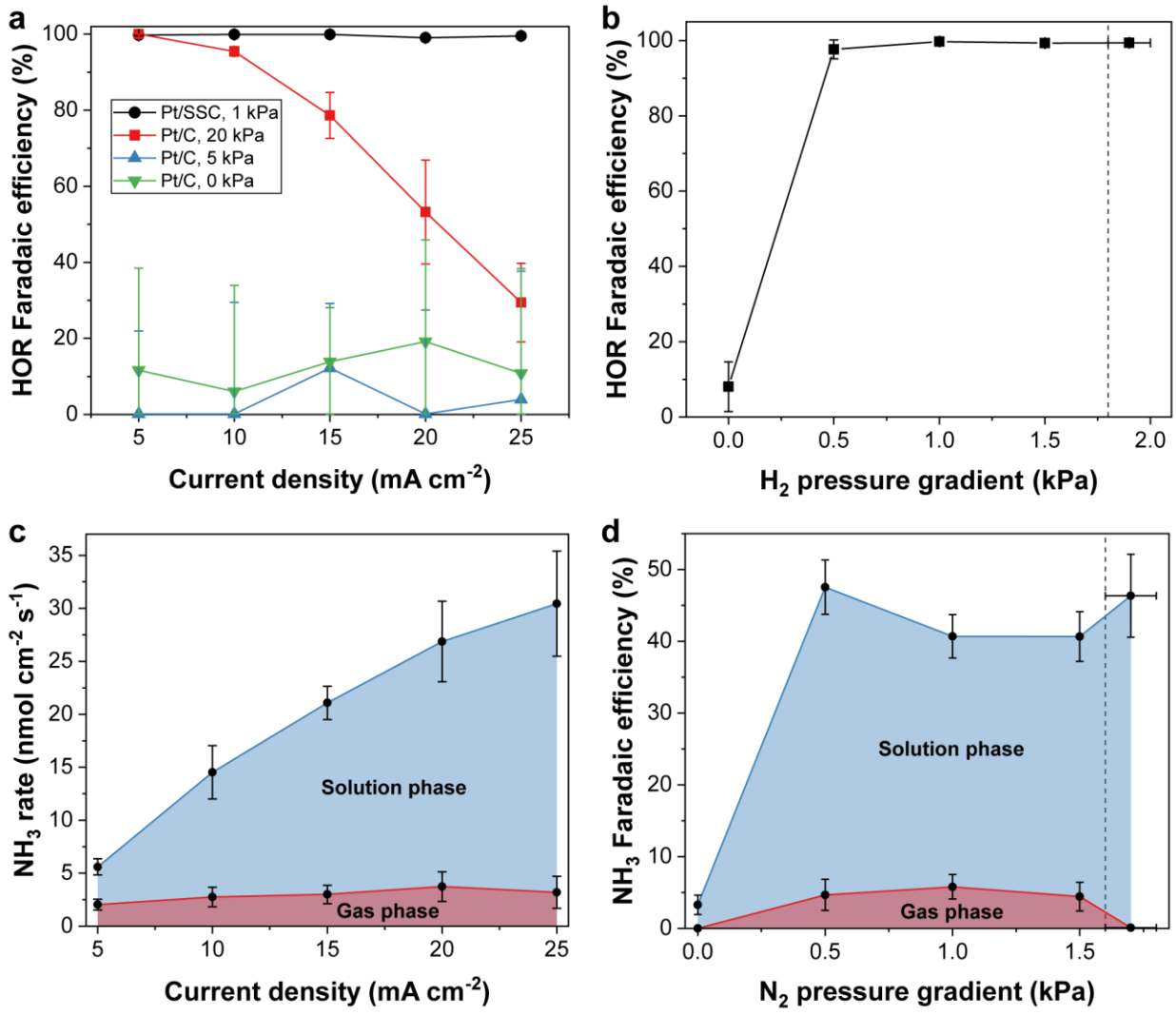

Fig. 3. Efficiency of the steel cloth-based GDEs for HOR and NRR. (**a**) Comparison of HOR Faradaic efficiency (FE) of Pt-coated steel cloths (Pt/SSC) and Pt-loaded carbon papers (Pt/C) at different pressure gradients across the GDEs. (**b**) Effect of pressure gradient across a Pt/SCC on HOR FE at 25 mA cm^{-2} applied current density. (**c**) Production rate of ammonia as a function of applied current density on steel cloth cathodes at a pressure gradient of 1 kPa across the steel cloth. Solution phase ammonia is found in the electrolyte while gas phase ammonia is found in the acid trap after the cell. (**d**) Effect of pressure gradient across a steel cloth cathode on FE toward NH_3 at 15 mA cm^{-2} applied current density. Vertical error bars in (**a**) and (**b**) represent a combination of

uncertainty in HOR quantification and standard deviation between experiments ($n \geq 2$), while in (**c**) and (**d**) they represent one standard deviation between multiple replicates of the same experiments ($n \geq 2$). Horizontal error bars in (**b**) and (**d**) represent the range of pressure gradient values required for gas flow through the SSCs. Raw data can be found in the in Supplementary Fig. 22 and Supplementary Tables 2-5. The dashed lines in (**b**) and (**d**) represent the onset of gas breakthrough in the SSC, which is the Laplace pressure. In all experiments, 7.2 coulombs of charge were passed to measure either HOR or NRR FE.

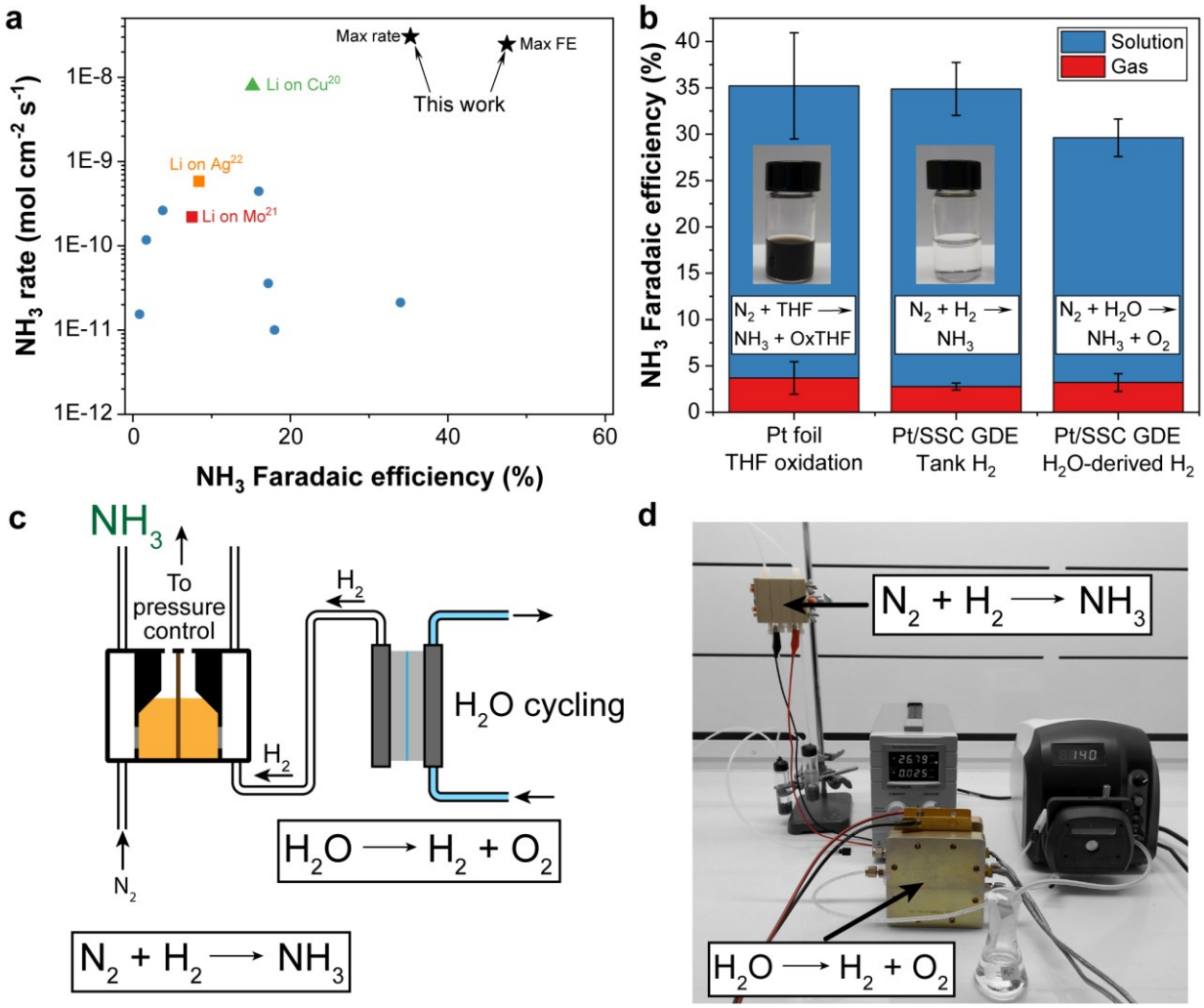

Fig. 4. Coupling of electrodes for a sustainable overall reaction. (**a**) Comparison of continuous ammonia production metrics at ambient conditions between our work and reported highest rates in nonaqueous electrolytes in the literature.[20–22] (**b**) Changes in Faradaic efficiency toward ammonia with different anode chemistries in experiments where 7.2 coulombs of charge were passed at an applied current density of 20 mA cm^{-2}, with 10 standard cubic centimeters per minute of gas flowing past the electrode, across which the pressure gradient is 1 kPa. Error bars represent the standard deviation of multiple replicates of the same experiment ($n \geq 2$). The insets show the anolyte after longer-term continuous operation at 20 mA cm^{-2} for one hour at respective anodes. The dark solution (Pt foil) contains poorly-defined tetrahydrofuran (THF) oxidation products,

while the clear solution (Pt/SCC) shows few signs of THF oxidation. (**c**) Schematic of an electrochemical Haber-Bosch (eHB) reactor coupled to a water-splitting reactor. (**d**) A photograph depicting a model of an eHB reactor coupled to a water electrolyzer, with the reactors highlighted.

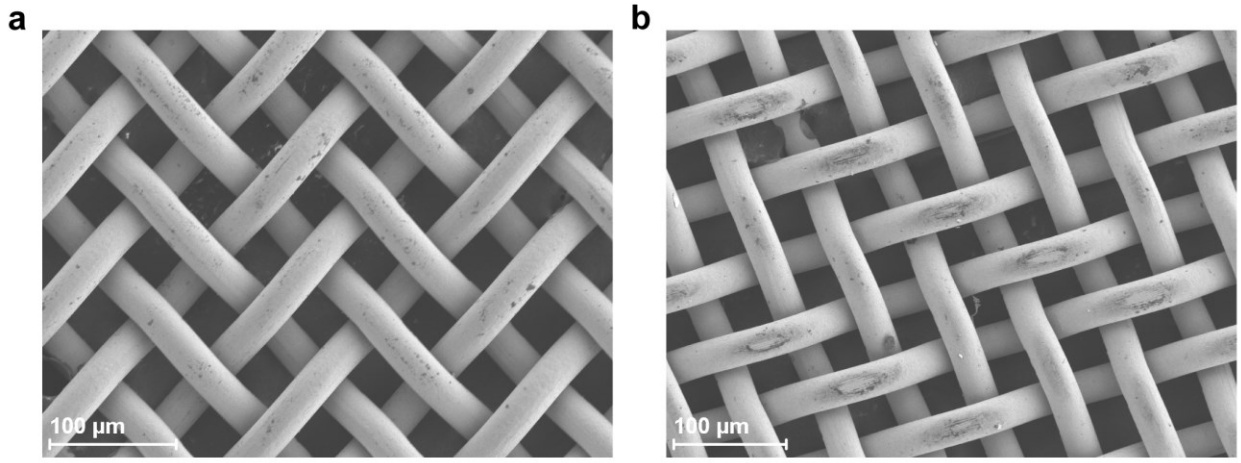

Extended Data Fig. 1. Scanning electron microscopy (SEM) images of stainless steel cloth electrodes. A Zeiss-Merlin HR-SEM with an HE-SE2 detector was used to collect images. (**a**) An image of a bare stainless steel cloth (SSC) (Supplementary Fig. 4). (**b**) An image of a nickel-coated SSC (Supplementary Fig. 5).

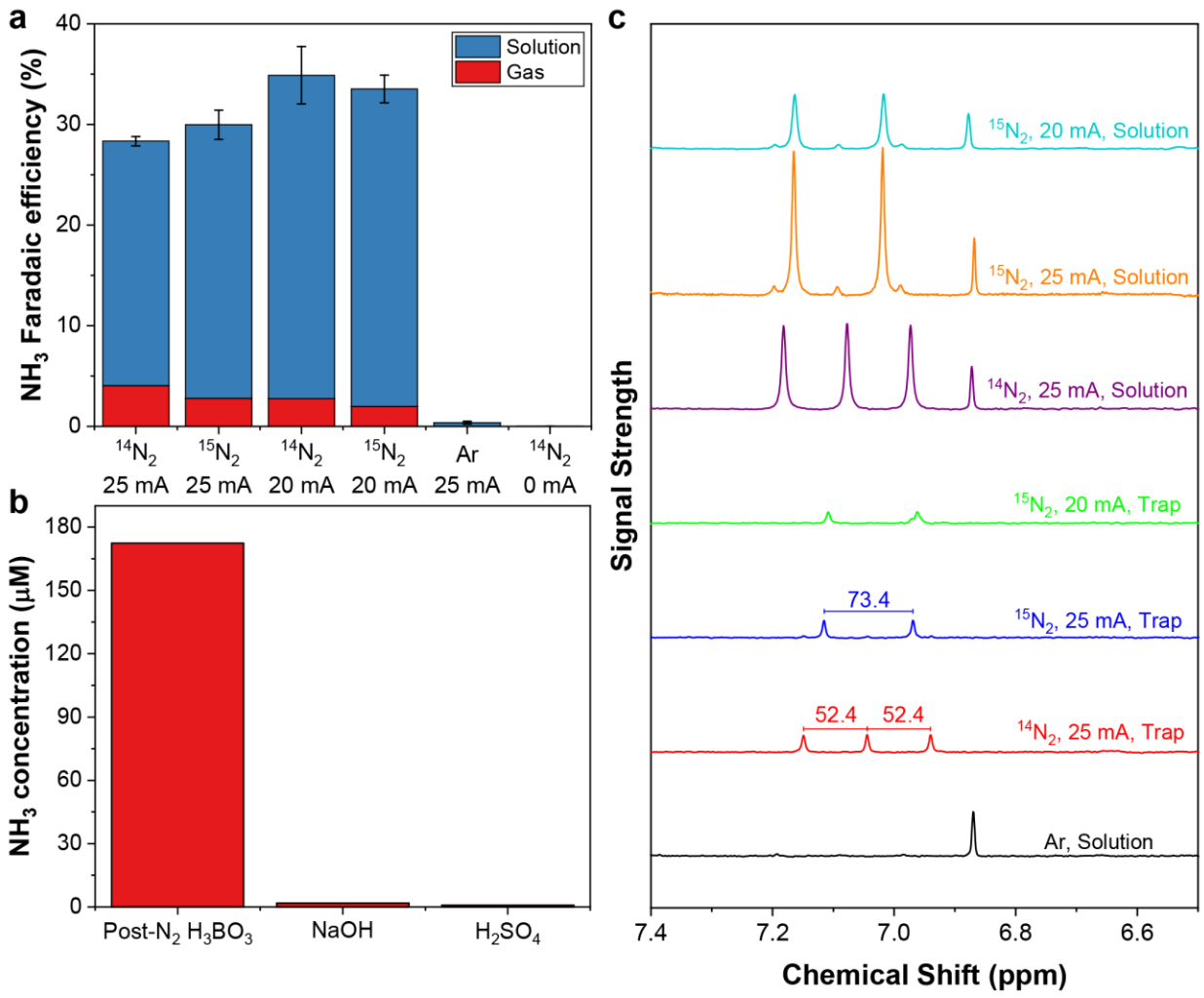

Extended Data Fig. 2. Control experiments confirming nitrogen reduction to ammonia. (**a**) A comparison between the Faradaic efficiency toward ammonia when various gases are fed to the cell. When using N_2 with different isotopic compositions, the ammonia yields are practically identical, which is a sign that N_2 reduction is responsible for ammonia formation.[21] There is little to no ammonia formed when Ar is used as the feed gas or in the absence of current. Vertical error bars represent the uncertainty in Faradaic efficiency quantification of a single experiment. (**b**) Amount of ammonia quantified in the base and acid traps used to clean the inlet gas, and the concentration of ammonia in a post-cell acid trap for comparison. (**c**) Unscaled NMR spectra of electrolyte and acid trap solutions. When $^{14}N_2$ is used as the feed gas, only a triplet from $^{14}NH_4^+$ is

detected in both the trap and solution, while both $^{15}NH_4^+$ and $^{14}NH_4^+$ are detected when $^{15}N_2$ is fed. ~92% of the NH_4^+ is $^{15}NH_4$, which suggests some $^{14}N_2$ contamination in the experiment, as the nominal isotopic content of the $^{15}N_2$ is 98%. The peaks shift slightly due to differences in solvent composition (THF-water mixtures). The peak at ~6.87 is from butylated hydroxytoluene (BHT) found in the THF. The 25 mA experiments were performed by using a 3-compartment cell with a platinum foil anode, while the 20 mA experiments used a cell with no separator between electrolyte compartments and a Pt/SSC anode.

Methods

Electrolyte preparation

Electrolyte solutions were prepared by dissolving 1 M of $LiBF_4$ (Sigma-Aldrich, 98+%) in molecular sieve-dried tetrahydrofuran (Acros Organics, 99+%, stabilized with BHT) to which ethanol (VWR International Koptek, anhydrous, 200 proof) was added to yield an ethanol concentration of 0.11 M. The obtained solution was centrifuged at 6000 rpm for 10 minutes to precipitate insoluble impurities. The clear solution was transferred to oven-dried glass vials and used within 12 hours of preparation. In experiments in which hydrogen oxidation is quantified, ferrocene (Alfa Aesar, 99%) was added to the solutions to yield a ferrocene concentration of ~0.25 M.

Preparation of platinum-coated steel cloths

Stainless steel cloths (McMaster-Carr, 304 stainless steel, 400x400 mesh) were electroplated with nickel followed by platinum (Supplementary Fig. 3). A Wood's nickel strike solution, which consists of 1 M $NiCl_2$ (Sigma-Aldrich) and 1 M HCl (Sigma-Aldrich) in water, was used to plate nickel onto the cloths (Supplementary Fig. 4). The cloth was used as the working electrode while a piece of nickel foil (Alfa Aesar, 99+%) was used as the soluble counter electrode in an undivided beaker cell. The cloth was pretreated by applying an oxidative current of 15 mA cm_{geom}^{-2} for 30 seconds, immediately after which a reductive current of 30 mA cm_{geom}^{-2} was applied for 5 minutes obtain a nickel-plated stainless steel cloth (Supplementary Fig. 5).

After striking the cloth with nickel, platinum can be deposited. The platinum plating solution used was a citrate-ammonium bath, containing 35 mM $(NH_4)_2PtCl_6$ (Alfa Aesar), 400 mM trisodium citrate (anhydrous, Beantown Chemical), and 75 mM NH_4Cl (Alfa Aesar). The nickel-stricken cloth was used as the working electrode; a piece of platinum foil was used as a soluble

counter electrode in a beaker cell, which was kept over a water bath at 90 °C. A constant reductive current of 10 mA (~5 mA cm_{geom}^{-2}) was applied to the cloth for 5 minutes. The platinum-coated cloths (Supplementary Figs. 6 and 7) were thoroughly rinsed with DI water to remove any ammonium containing compounds from the surface and dried at 80 °C in air prior to use.

Gas diffusion electrode experiments

Experiments were performed in 3-compartment cells (Supplementary Figs. 15 and 16), in which working and counter electrode compartments were separated by a Daramic 175 separator; all cell parts were oven-dried at 80 °C before use. The working electrode was a piece of stainless steel cloth in nitrogen reduction experiments or a piece of platinum-coated stainless steel cloth in hydrogen oxidation experiments. The working electrode was fixed between the working electrode compartment and a gas compartment. The working gas (e.g. N_2 or H_2) was flowed first through a vial containing THF to saturate the gas with THF, followed by the gas compartment of the electrochemical cell; the gas was slightly pressurized by a water column at the outlet of the gas compartment (Supplementary Fig. 17). In experiments where propylene carbonate-based electrolyte was used, the vial contained propylene carbonate instead of THF.

1.75 mL of electrolyte was added to each electrode compartment, for a total electrolyte volume of 3.5 mL. Note that this is the volume of electrolyte added to each compartment and may not be the final electrolyte volume due to electrolyte evaporation. At this point, a pressure gradient was established across the working electrode due to the fact that the electrolyte compartment is at atmospheric pressure while the gas compartment is at positive pressure due to the water column at the compartment outlet; this pressure gradient prevents electrolyte flow into the gas compartment and establishes a robust gas-electrolyte interface (Supplementary Fig. 2). Initially, the height of the water column was chosen to redirect gas flow into the electrolyte compartment. Gas was flowed

into the electrolyte for 10 minutes at 10 standard cubic centimeters per minute (sccm) to saturate the solution with the gas. The height of the water column was then lowered to obtain the desired pressure gradient across the SSC while maintaining flow past the SSC. In certain experiments, the flowrate of the gas past the electrode was also decreased at this stage (Supplementary Fig. 10). A constant current was then applied to the cell; in most experiments, 7.2 coulombs of charge were applied irrespective of current density.

For nitrogen reduction experiments, an additional vial containing 2 mL of 0.1 M H_3BO_3 (Alfa Aesar, 99.99%) was added between the gas compartment and the water column to capture any gas phase ammonia (Supplementary Fig. 17). To quantify ammonia, the catholyte was diluted to 100 mL in a volumetric flask in water, after which the obtained solutions were either used as-is or diluted 2- or 4-fold further for ammonia quantification via a colorimetric assay (Supplementary Fig. 18). The boric acid trap was quenched with 500 μL of 0.4 M NaOH before being diluted to 25 mL in a volumetric flask. The ammonia content in the trap-derived solution was quantified via a colorimetric assay without further dilution.

For some hydrogen oxidation experiments, the electrolyte contained ferrocene at a concentration of ~0.25 M, the oxidation of which was used to estimate the FE toward hydrogen oxidation (see Supplementary Discussion). In mass-balance closure and eHB cell experiments, the electrolyte was unchanged from the one used in nitrogen reduction experiments.

Ammonia quantification

Ammonia in prepared samples was quantified using a modification of the salicylate method,[43] which has been described in detail in prior work.[20] Briefly, two solutions were prepared: the hypochlorite solution, which contains 1% NaOCl (Sigma-Aldrich) in 0.4 M NaOH in water, and the salicylate solution, which contains 2.5 M of purified sodium salicylate (Sigma-Aldrich)

and 0.5 mM sodium nitroprusside (99-102%, Alfa-Aesar) in water. To a 2 mL sample containing ammonia, 280 μL of the hypochlorite solution was added, followed by 280 μL of the salicylate solution. The solution was then mixed and left in the dark to evolve color for approximately 2 hours. The absorbance spectrum of the resulting solution was measured using a spectrophotometer; the relevant signal for quantification was taken to be difference between the absorbance of the solution at 650 and 475 nm.[20] Calibration curves were prepared by using solutions with known concentrations of NH_4Cl in water (Supplementary Fig. 19). Quantification via colorimetric assay was found to give results consistent with those obtained by NMR (Supplementary Fig. 20).

Nitrogen reduction control experiments

Nitrogen reduction to ammonia at SSC cathodes was confirmed by varying the feed gas in NRR experiments (Extended Data Fig. 2). All feed gases passed through three solutions before entering the cell to purify and prepare the gas. First, the gases were passed through 0.1 M NaOH to capture any NO_x in the gases, then through 0.05 M H_2SO_4 to capture any NH_3, followed by THF with sieves to capture water in the gaseous stream and to saturate the gas with THF. Initially, 10 sccm of argon gas were passed through all three solutions to remove air, which contains $^{14}N_2$ and O_2. Then, 5 sccm of the desired gas – Ar (Airgas), $^{14}N_2$ (Airgas), or $^{15}N_2$ (Cambridge Isotope Laboratories) – were passed through the solutions and fed to the cell for nitrogen reduction experiments.

Two architectures were used to confirm nitrogen reduction. In one set of experiments, a 3-compartment cell (Supplementary Fig. 15) with a SSC cathode, Pt foil anode, and a Daramic separator was used; 25 mA of current were applied to the cell for 290 seconds in these experiments. In the second set of experiments, a 4-compartment cell (Fig. 4d) with a SSC cathode, Pt/SSC

anode, and no separator was used; in this configuration, 5 sccm of H_2 (Airgas) were fed to the anode. 20 mA of current were applied for 360 seconds in these experiments.

The catholyte from the 3-compartment cell experiments, all the electrolyte from the 4-compartment cell experiments, and the acid traps were acidified with 0.05 M H_2SO_4 in water to convert all NH_3 to NH_4^+. NMR spectra of the obtained solutions were taken with solvent suppression on a Bruker Avance Neo 500.18 MHz spectrometer (Extended Data Fig. 2c). The ammonia content of the solutions was quantified via the colorimetric assay; the measured concentrations of ammonia were found to be consistent with those measured by NMR (Supplementary Fig. 20).

Hydrogen oxidation quantification

To quantify the HOR FE, an excess of ferrocene (~0.25 M) was added to the electrolyte prior to electrolysis. As ferrocene is thermodynamically more difficult to oxidize than H_2, but easier than THF (Fig. 1b), any applied current would first oxidize H_2, assuming the oxidation is kinetically facile, followed by ferrocene, once HOR is diffusion limited. After application of current in HOR experiments using Pt/SSC anodes, the anolyte was diluted to 10 mL with N_2-purged water. The produced cloudy orange mixture was extracted with N_2-purged hexanes three times. The obtained solution was centrifuged for improved phase separation. The ferrocenium content of the produced clear aqueous solutions was quantified via UV-vis spectroscopy by using a combination of the visible (619 nm) and UV (255 nm) ferrocenium absorption peaks (Supplementary Fig. 21). The concentration of ferrocenium in solution was then used to estimate the maximum value of HOR FE. For a detailed discussion of the method, see the Supplementary Methods and Discussion.

For experiments at low flowrates and high currents (i.e. at high conversions), the HOR FE was also computed by estimating the hydrogen flowrate out of the gas compartment and by using a hydrogen mass balance over the gas compartment (Supplementary Figs. 9 and 11). The results were consistent with those obtained via the ferrocene-based method. For a detailed discussion of the method, see the Supplementary Methods.

Data availability: The data that support the plots within this paper and other findings of this study are available from the corresponding author upon request.

Image processing software: Data were plotted in Origin 2018b (9.5). The plots obtained from Origin were compiled in Adobe Illustrator v 23.0. Diagrams were drawn in Adobe Illustrator. Photographs in the main text and Supplementary Information figures were trimmed and contrasted by using GNU Image Manipulation Program (GIMP) v 2.10.12.

References

1. Schiffer, Z. J. & Manthiram, K. Electrification and Decarbonization of the Chemical Industry. *Joule* **1**, 10–14 (2017).
2. Yan, M., Kawamata, Y. & Baran, P. S. Synthetic Organic Electrochemistry: Calling All Engineers. *Angew. Chemie Int. Ed.* **57**, 4149–4155 (2018).
3. Chen, J. G. *et al.* Beyond fossil fuel–driven nitrogen transformations. *Science (80-.).* **360**, eaar6611 (2018).
4. Soloveichik, G. Electrochemical synthesis of ammonia as a potential alternative to the Haber–Bosch process. *Nat. Catal.* **2**, 377–380 (2019).
5. Shipman, M. A. & Symes, M. D. Recent progress towards the electrosynthesis of ammonia from sustainable resources. *Catal. Today* **286**, 57–68 (2017).
6. Comer, B. M. *et al.* Prospects and Challenges for Solar Fertilizers. *Joule* **3**, 1578–1605 (2019).
7. Suryanto, B. H. R. *et al.* Challenges and prospects in the catalysis of electroreduction of nitrogen to ammonia. *Nat. Catal.* **2**, 290–296 (2019).
8. Foster, S. L. *et al.* Catalysts for nitrogen reduction to ammonia. *Nat. Catal.* **1**, 490–500 (2018).
9. Jiao, F. & Xu, B. Electrochemical Ammonia Synthesis and Ammonia Fuel Cells. *Adv. Mater.* **31**, 1805173 (2019).
10. Davis, S. J. *et al.* Net-zero emissions energy systems. *Science (80-.).* **360**, eaas9793 (2018).
11. Liu, X., Jiao, Y., Zheng, Y., Jaroniec, M. & Qiao, S.-Z. Building Up a Picture of the Electrocatalytic Nitrogen Reduction Activity of Transition Metal Single-Atom Catalysts. *J. Am. Chem. Soc.* **141**, 9664–9672 (2019).

12. Peters, B. K. *et al.* Scalable and safe synthetic organic electroreduction inspired by Li-ion battery chemistry. *Science (80-.).* **363**, 838–845 (2019).

13. Matthessen, R., Fransaer, J., Binnemans, K. & De Vos, D. E. Electrocarboxylation: towards sustainable and efficient synthesis of valuable carboxylic acids. *Beilstein J. Org. Chem.* **10**, 2484–2500 (2014).

14. Möhle, S. *et al.* Modern Electrochemical Aspects for the Synthesis of Value-Added Organic Products. *Angew. Chemie - Int. Ed.* **57**, 6018–6041 (2018).

15. McEnaney, J. M. *et al.* Ammonia synthesis from N_2 and H_2O using a lithium cycling electrification strategy at atmospheric pressure. *Energy Environ. Sci.* **10**, 1621–1630 (2017).

16. Kim, K., Chen, Y., Han, J.-I., Yoon, H. C. & Li, W. Lithium-mediated ammonia synthesis from water and nitrogen: a membrane-free approach enabled by an immiscible aqueous/organic hybrid electrolyte system. *Green Chem.* (2019) doi:10.1039/C9GC01338E.

17. Kim, K. *et al.* Electrochemical Synthesis of Ammonia from Water and Nitrogen: A Lithium-Mediated Approach Using Lithium-Ion Conducting Glass Ceramics. *ChemSusChem* **11**, 120–124 (2018).

18. Kim, K. *et al.* Lithium-Mediated Ammonia Electro-Synthesis: Effect of CsClO 4 on Lithium Plating Efficiency and Ammonia Synthesis. *J. Electrochem. Soc.* **165**, F1027–F1031 (2018).

19. McEnaney, J. M. *et al.* Electro-thermochemical Li cycling for NH_3 synthesis from N_2 and H_2O. 1–11 (2019).

20. Lazouski, N., Schiffer, Z. J., Williams, K. & Manthiram, K. Understanding Continuous

Lithium-Mediated Electrochemical Nitrogen Reduction. *Joule* **3**, 1127–1139 (2019).

21. Andersen, S. Z. *et al.* A rigorous electrochemical ammonia synthesis protocol with quantitative isotope measurements. *Nature* **570**, 504–508 (2019).

22. Tsuneto, A., Kudo, A. & Sakata, T. Lithium-mediated electrochemical reduction of high pressure N_2 to NH_3. *J. Electroanal. Chem.* **367**, 183–188 (1994).

23. Schwalbe, J. A. *et al.* A Combined Theory-Experiment analysis of the Surface Species in Lithium Mediated NH3 Electrosynthesis. *ChemElectroChem* celc.201902124 (2020) doi:10.1002/celc.201902124.

24. Singh, A. R. *et al.* Strategies toward Selective Electrochemical Ammonia Synthesis. *ACS Catal.* **9**, 8316–8324 (2019).

25. Gibanel, F., López, M. C., Royo, F. M., Santafé, J. & Urieta, J. S. Solubility of nonpolar gases in tetrahydrofuran at 0 to 30°C and 101.33 kPa partial pressure of gas. *J. Solution Chem.* **22**, 211–217 (1993).

26. Bard, A. J. & Faulkner, L. R. *Electrochemical Methods. Fundamentals and Applications*. (John Wiley & Sons, Inc, 2001).

27. Zhou, F. *et al.* Electro-synthesis of ammonia from nitrogen at ambient temperature and pressure in ionic liquids. *Energy Environ. Sci.* **10**, 2516–2520 (2017).

28. Mathur, V. & Crawford, J. Fundamentals of Gas Diffusion Layers in PEM Fuel Cells. *Recent Trends Fuel Cell Sci. Technol.* **400**, 116–128 (2007).

29. Litster, S. & McLean, G. PEM fuel cell electrodes. *J. Power Sources* **130**, 61–76 (2004).

30. Ripatti, D. S., Veltman, T. R. & Kanan, M. W. Carbon Monoxide Gas Diffusion Electrolysis that Produces Concentrated C_2 Products with High Single-Pass Conversion. *Joule* **3**, 240–256 (2018).

31. Ren, S. *et al.* Molecular electrocatalysts can mediate fast, selective CO_2 reduction in a flow cell. *Science (80-.).* **365**, 367–369 (2019).

32. Higgins, D., Hahn, C., Xiang, C., Jaramillo, T. F. & Weber, A. Z. Gas-Diffusion Electrodes for Carbon Dioxide Reduction: A New Paradigm. *ACS Energy Lett.* **4**, 317–324 (2019).

33. Burdyny, T. & Smith, W. A. CO_2 reduction on gas-diffusion electrodes and why catalytic performance must be assessed at commercially-relevant conditions. *Energy Environ. Sci.* **12**, 1442–1453 (2019).

34. Weng, L. C., Bell, A. T. & Weber, A. Z. Modeling gas-diffusion electrodes for CO_2 reduction. *Phys. Chem. Chem. Phys.* **20**, 16973–16984 (2018).

35. Tran, C., Yang, X.-Q. & Qu, D. Investigation of the gas-diffusion-electrode used as lithium/air cathode in non-aqueous electrolyte and the importance of carbon material porosity. *J. Power Sources* **195**, 2057–2063 (2010).

36. Balaish, M., Kraytsberg, A. & Ein-Eli, Y. Realization of an artificial three-phase reaction zone in a Li-Air battery. *ChemElectroChem* **1**, 90–94 (2014).

37. Gourdin, G., Xiao, N., McCulloch, W. & Wu, Y. Use of Polarization Curves and Impedance Analyses to Optimize the 'triple-Phase Boundary' in K-O_2 Batteries. *ACS Appl. Mater. Interfaces* **11**, 2925–2934 (2019).

38. Santamaria, A. D., Das, P. K., MacDonald, J. C. & Weber, A. Z. Liquid-water interactions with gas-diffusion-layer surfaces. *J. Electrochem. Soc.* **161**, F1184–F1193 (2014).

39. Morgan, E. R., Manwell, J. F. & McGowan, J. G. Sustainable Ammonia Production from U.S. Offshore Wind Farms: A Techno-Economic Review. *ACS Sustain. Chem. Eng.* **5**, 9554–9567 (2017).

40. Greenlee, L. F., Renner, J. N. & Foster, S. L. The Use of Controls for Consistent and Accurate Measurements of Electrocatalytic Ammonia Synthesis from Dinitrogen. *ACS Catal.* **8**, 7820–7827 (2018).

41. Kibsgaard, J., Nørskov, J. K. & Chorkendorff, I. The Difficulty of Proving Electrochemical Ammonia Synthesis. *ACS Energy Lett.* **4**, 2986–2988 (2019).

42. Inc., N. *Equipment design and cost estimation for small modular biomass systems, synthesis gas cleanup and oxygen separation equipment*. *NREL Subcontract report* http://www.nrel.gov/docs/fy06osti/39946.pdf (2006).

43. Verdouw, H., Van Echteld, C. J. A. & Dekkers, E. M. J. Ammonia determination based on indophenol formation with sodium salicylate. *Water Res.* **12**, 399–402 (1978).

Acknowledgements: We thank Matt Wolski of Daramic for providing us with polyporous separator samples. Funding: This material is based upon work supported by the National Science Foundation under Grant No. 1944007 and the MIT Energy Initiative (MITEI) Seed Fund. N.L. acknowledges support by the National Science Foundation Graduate Research Fellowship under Grant No. 1122374.

Author Contributions: Conceptualization, N.L. and K.M. Methodology, N.L. Methodology – Coupling to water splitting, M.L.G. Investigation, N.L. Validation, M.C. Writing – Original Draft, N.L. Writing – Review & Editing, N.L., M.C., K.W. and K.M. Supervision, K.M.

Competing interests: Authors declare no competing interests.